### Tunable Nonlinear Topological Insulator for Acoustic Waves

Amir Darabi\* and Michael J. Leamy<sup>†</sup>

Inspired by the quantum spin Hall effect (QSHE), we propose the first two-dimensional tunable nonlinear topological insulator for acoustic waves that activates simply by inputting energy. Tunability is derived from an energy-dependent topological band structure, where the topological bandgap opens intrinsically using nonlinear elements. A discrete hexagonal unit cell (composed of six masses, twelve linear, and three nonlinear springs) is repeated to construct a phononic system exhibiting topological character. The corresponding band structure of the proposed hexagonal unit cell is obtained analytically using Bloch's theorem and zone folding techniques, which documents double degenerate Dirac cones. Breaking of inversion symmetry creates energy-dependent topologically protected bandgaps, with topologically protected edge states (TPES) robust against back-scattering at arbitrary interfaces of two structures with opposite Chern numbers. The proposed topological insulator can be a stepping-stone platform towards building tunable acoustic devices, interconnects, and electroacoustic integrated circuits.

Starting with electronic states in condensed matter physics [1–5], and then later in electromagnetic materials [6–9], and still later for mechanical waves in phononic systems [10–13], the investigation of topological insulators (TI) has experienced growing attention in the last several years. These topological structures are induced by quantum Hall and quantum spin Hall effects, or their analogs, and have the potential to protect edge states against back-scattering at sharp interfaces, defects and disorders.

Topologically protected edge states (TPES) have been explored in mechanical systems to control statical states [10, 14-19] and dynamical waves [12, 20] immune to back-scattering. These TIs can be categorized into two quantum-analogous categories: active devices to realize chiral edge states mimicking the quantum Hall effect (QHE) [13, 21, 22], and passive devices that realize helical edge states mimicking the quantum spin Hall effect (QSHE) [11]. To realize chiral edges states requires breaking time-reversal (T-symmetry) by employing, for example, a weak magnetic field [23]; gyroscopes or rotating frames yielding resultant Coriolis forces [24–26]; or varying material properties in time and space [27–30]. On the other hand, for passive devices, helical edge states require only breaking inversion symmetry [31]. These devices do not require energy input, feature both forwardand backward-propagating edge modes, and generally maintain T-symmetry. This group of TIs has been explored using different sizes of steel inclusions in water [32], two-scale parts in thin plates [11], periodically arranged resonators [33–35], or balls and linear springs in discrete systems [36, 37]. It should be noted that TIs are characterized by a topological measure (e.g., Chern number) [38, 39], whose quantized value for each material, and more specifically its difference across an interface, dictates the number of edges states [1].

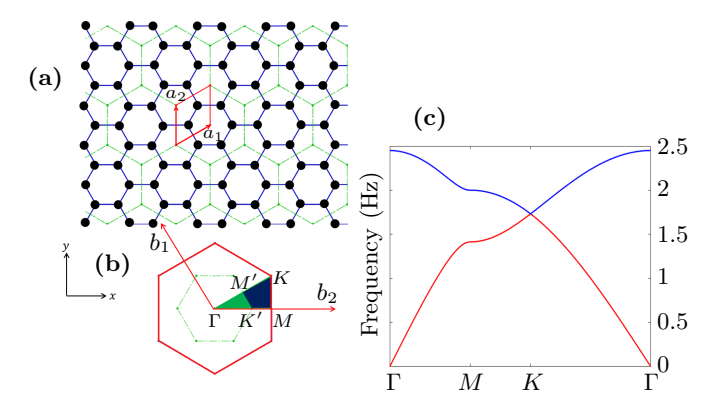


FIG. 1. Phononic crystal with Dirac cones.(a) Schematic of the phononic crystal composed of masses connected using linear springs. (b) Schematic of the first Brillouin zone for the system with two masses (larger red hexagon corresponding to the red hexagonal honeycomb in Fig. 1(a)) and the system with six masses (smaller green hexagon corresponding to the green hexagonal unit cell in Fig. 1(a)). (c) Band structure along the first irreducible Brillouin zone perimeters for the unit cell with two masses in Fig. 1(a), documenting a Dirac cone at f = 1.6Hz.

One of the current challenges in applying mechanical TIs to solve real-world applications is their lack of tunablity, and thus difficult adaption to functional needs. To overcome this issue, designing programmable TIs has gained attention for potential application in acoustic devices, interconnects, and electroacoustic circuits [40]. Recent studies have proposed programmable TIs for acoustical systems by, i) rotating each unit cell using computercontrolled motors to achieve desired angles [41], ii) employing a magnetic fluid to fill the unit cell cavity [42], or iii) fixing the free inclusion in a hexagonal structure [43]. Although all of the reviewed reconfigurable TIs are capable of generating back-scattering immune TPES, they either change the geometry of the structure or require an external element to control the condition of the system. Another possible strategy for designing a reconfigurable structure is to employ nonlinear elements for mechanical waves. These nonlinear elements were em-

<sup>\*</sup> Woodruff School of Mechanical Engineering, Georgia Institute of Technology, Atlanta, GA

 $<sup>^\</sup>dagger$  Woodruff School of Mechanical Engineering, Georgia Institute of Technology, Atlanta, GA; michael.leamy@me.gatech.edu

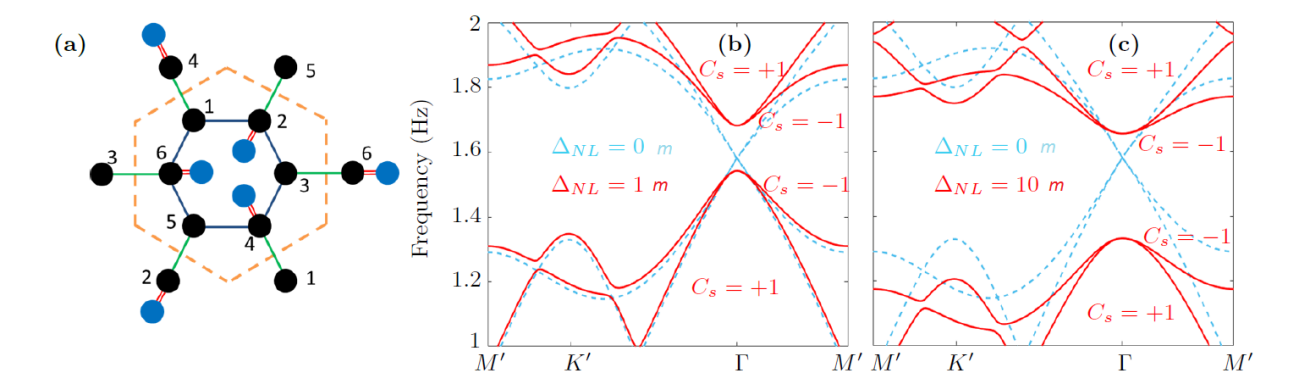


FIG. 2. Topological demonstration of a hexagonal unit cell. (a) A hexagonal unit cell (marked with orange dashed-lines) composed of six masses (black circles with  $m_1 = 1.2kg$ ) connected using linear stiffness (dark blue springs with  $k_{L1} = 1N/m$ , and green springs with  $k_{L2} = 1.25N/m$ ), three resonant masses (light blue circles with  $m_2 = 0.6kg$ ) coupled to masses 2,4, and 6 via purely cubic stiffness ( $k_{NL} = 1N/m^3$ ). Numerically-computed band structure using the edges of the first Brillouin zone with corresponding spin Chern numbers, (b) when no energy is in the system (plotted in light blue), and when displacement of the nonlinear springs is 1 (plotted in red), and (c) when no energy is in the system (plotted in light blue), and when displacement of the nonlinear springs is 10 (plotted in red).

ployed in the past few years to design robust topological insulators for photonic [44] and electronic [45] structures. These nonlinear configurations provide energy-dependent dispersion relationships [46–49], which are sufficient to achieve a passive and tunable TI. Most recently, Pal et al. proposed a linear lattice with a topological bandgap, and studied the robustness of the system in the presence of weakly nonlinear springs [50]. Furthermore, Chaunsali et al. proposed a new self-induced structure for topological transition of acoustic waves by employing stiffening and softening nonlinear springs [51]. They showed that the proposed lattice makes a topological transition simply by altering the excitation amplitude.

In this letter we propose and numerically study a tunable mechanical topological insulator exhibiting topologically-protected edge states through a nonlinearity-induced opening of a topological bandgap. At zero energy, the gap is closed and it is only when energy is present that the gap opens. This can be contrasted to the study in [50] where the robustness of the TPES already present in a linear system were considered in light of potential nonlinearities. Here, the nonlinear configuration of the structure provides remote tuning of the band structure, which can improve and boost the bandwidth of the structure. Our tunable system consists of a hexagonal lattice incorporating six masses connected using linear springs, where three of the masses are coupled to internal resonators via essentially nonlinear springs. Energy-dependent band structure exhibits double degenerate bands at the Dirac point. Upon energy input, inversion symmetry is broken; thus, a topologicallyprotected bandgap is created, and behavior analogous to the quantum spin Hall effect results.

#### I. RESULTS

### A. Designing a meta-structure exhibiting Dirac

In the first step aimed at designing a tunable mechanical TI, we tailor the band structure of a hexagonal honeycomb unit cell to enable separation of two doubly-folded Dirac cones. Figure 1(a) depicts the schematic of a shear lattice (i.e., supporting transverse displacements) composed of masses  $(m_1 = 1.2 \text{ kg})$  coupled using purely linear springs  $(k_{L1} = 1 \text{ N/m})$ , while Fig. 1(b) denotes the primitive unit cell (marked by red dashed lines). This simple system exhibits intersecting Dirac cones, where two distinct wave modes meet at one point. Its band structure is computed using the edges of the irreducible Brillouin zone (IBZ) (see Fig. 1(b), blue outline). Figure 1(c) displays the resulting band structure documenting a two-fold degeneracy at the K point  $(f \approx 1.6 \text{ Hz})$ .

## B. Achieving QSHE analog by breaking mirror symmetry

Next, a zone folding technique [52, 53], together with an extended unit cell with broken symmetry (see next section) including six masses denoted by green hexagons in Fig. 1(a), is considered to achieve doubly-degenerate Dirac cones at the  $\Gamma$  point. Figure 1(b) also depicts the irreducible Brillouin zone (IBZ) for the new unit cell (green outline) and the location of special symmetry points. As shown, the K-point in the larger hexagon (for a unit cell with two masses) will be folded into the center of the smaller hexagon (for a unit cell with six masses). The next step toward realizing the QSHE analog requires opening a topologically protected gap between the four

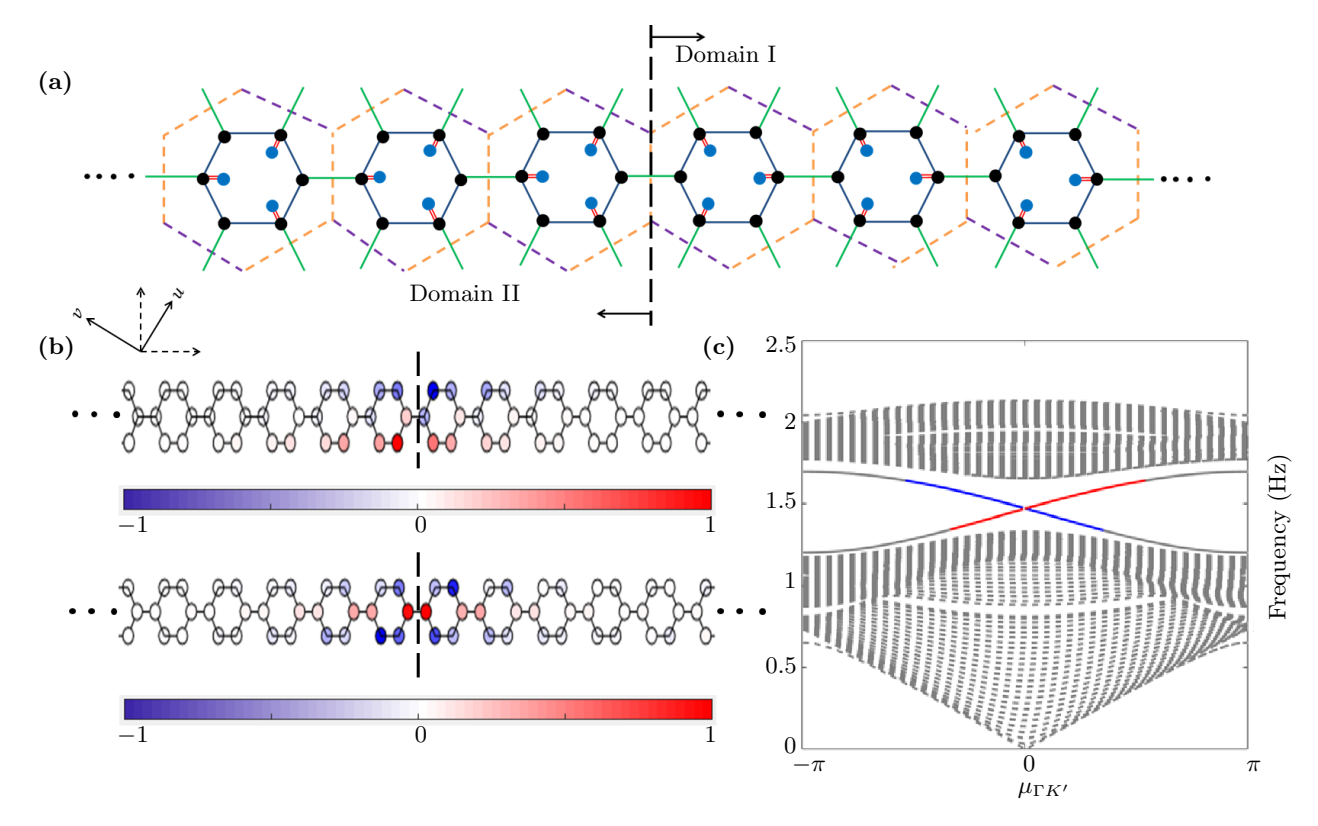


FIG. 3. **Topological interface modes.** (a) Schematic of a periodic strip in the horizontal direction with an interface between two domains (i.e., crystals) with opposite Chern numbers. On the left domain, masses 2,4, and 6 are connected by cubic springs. On the right domain, masses 1,3, and 5 are connected by cubic springs. This depicted structure is repeated along the direction perpendicular to the purple edges of the strip to represent a 2-D structure (i.e., the *u*-direction). (b) Corresponding edge mode shapes at  $\mu_{\Gamma K'} = \pi/6$ , documenting localization at the interface of two domains with opposite Chern numbers. (c) Numerically computed band structure of the topologically-protected phononic structure displayed in Fig. 3(a). Gray areas depict bulk bands, red dashed line depicts the forward edge mode, and blue the backward edge mode, respectively. Mode shapes are normalized with respect to the maximum and minimum displacements of the cell.

Dirac modes by breaking inversion symmetry (i.e.,  $C_6$  to  $C_3$ ). This is achieved by connecting resonating masses to half of the hexagonal unit cell masses with essentially nonlinear springs. In order to justify the zone folding technique, linear springs coupling each hexagonal unit cell are introduced with  $k_{L2} = 1.25 \ N/m$  (green springs in Fig. 2). As shown in Fig. 2(a), the final unit cell is now composed of the six original masses, in which three of them (masses numbered 2, 4, and 6) are attached to resonators (m = 0.6 kg) with nonlinear springs  $(k_{NL} = 1 \ N/m^3)$ . These springs have no linear stiffness, and are commonly realized using strings with zero pretension, or other means. Figures 2(b)-(c) plot the band structure of the system in Fig.2(a) for several input energies. As illustrated, in the absence of excitation energy, no bandgap is observed; however, upon energy input, a topologically-protected frequency bandgap is opened at the location of the separated Dirac modes. In addition, with further energy input, the bandgap widens until it reaches a maximum possible value (see Fig. 2(c)). At this condition, the nonlinear springs behave as rigid connections in comparison to the linear springs, and inputting more energy does not change the relative displacement

between the lattice mass and the nonlinear resonator. The corresponding eigenstates of the four distinct modes that bound the bandgap are depicted in Fig. 2(d), each depicting the influence of the nonlinear resonator. For each of the Dirac modes in Fig. 2(b)-(c), the corresponding spin Chern numbers are computed numerically to be  $C_s=\pm 1$ . Note that, if masses numbered 1, 3, and 5 are connected to nonlinear resonators instead of 2, 4, and 6, all spin Chern numbers in Fig.2(b)-(c) will be reversed. Supplementary Notes 1 and 2 provide further details on the generation of the band structures, mode shapes, and computation of spin Chern numbers.

## C. Observing topologically protected interface waves

The most intriguing attribute of topological edge states is their immunity to back-scattering at sharp edges and interfaces. If two structures with opposite signs in their spin Chern numbers share an interface (i.e., one structure with nonlinear resonators attached to mass 2, 4, and 6 and one with nonlinear resonators attached to mass 1,3,

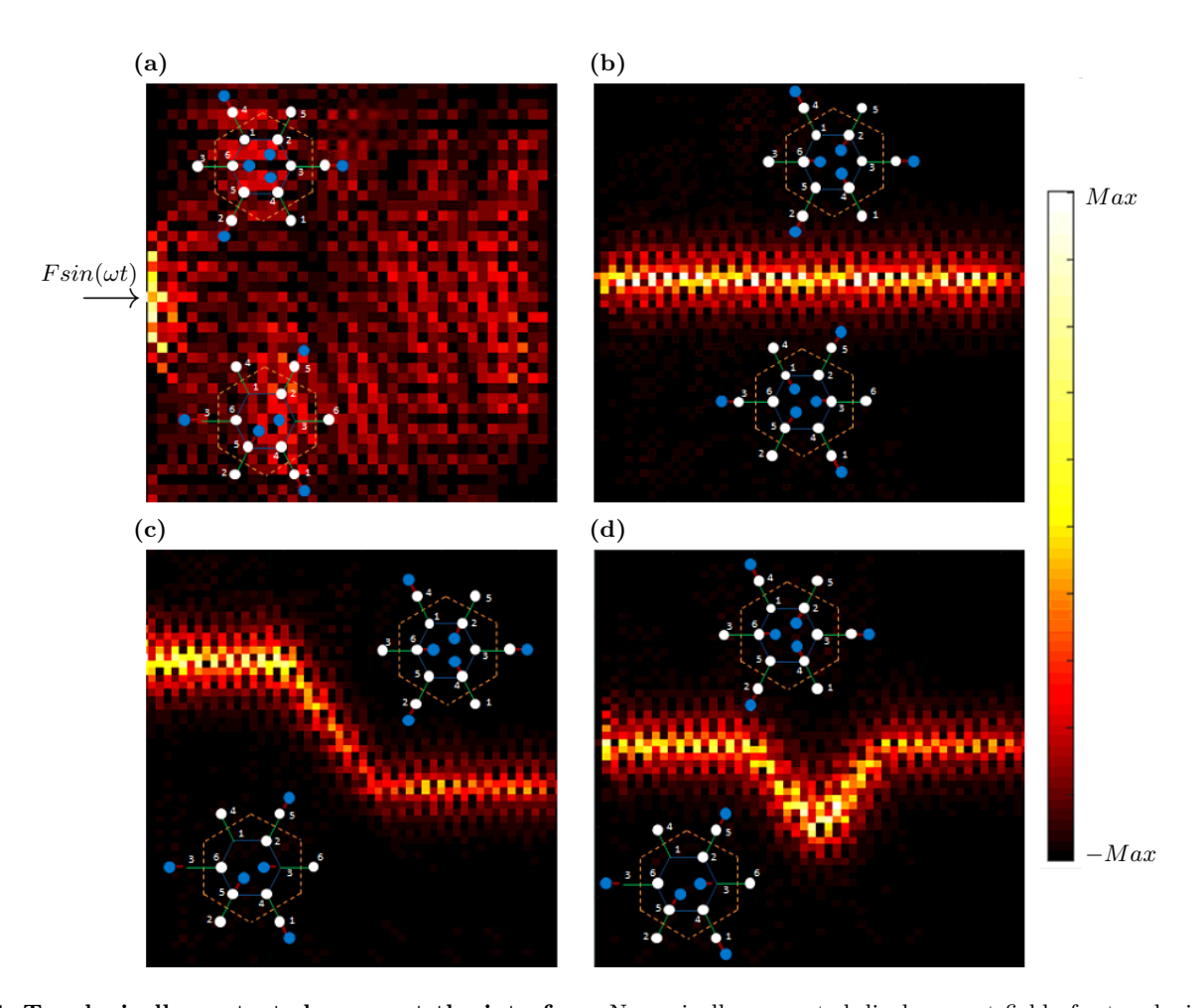


FIG. 4. Topologically protected waves at the interface. Numerically-computed displacement field of a topological edge state at the interface of two domains with opposite spin Chern numbers excited by a source at frequency 1.35 Hz for a, (a) horizontal interface when F = 1N, (b) horizontal interface when F = 100N, (c) zigzag-shaped interface when F = 100N, and (d) triangular-shaped interface when F = 100N, documenting immune to back-scattering wave propagation along the interfaces for a large force amplitude and wave propagation inside the Bulk for a small force amplitude. For all the depicted cases, a source is located on the left side of the structure and the displacements are normalized with respect to the source displacement.

and 5), two helical edge modes will be present at the interface ( $|\Delta C_s| = 2$ ), one forward-moving TPES and one backward-moving TPES, according to the bulk-edge correspondence principle [54, 55]. To demonstrate this, a finite strip of twenty unit cells is considered, which then repeats indefinitely in the  $\pm u$ -directions. Figure 3(a) depicts the schematic of the strip including two subdomains of ten cells each with opposite Chern numbers. On the right half of the strip, all masses with the indices of 2,4, and 6 are connected to nonlinear resonators, while on the left half only masses 1,3, and 5 are connected to nonlinear resonators, respectively. Figure 3(b)-(c) document the band structure and the corresponding mode shapes associated with the interface states for large energy input ( $\Delta_{NL} > 10$ , for more details on the calculation of this number are provided in Supplementary Note 1). These figures clearly reveal the existence of two edge modes starting from near the bulk modes on top to the bulk modes on the bottom at the location of the topologically

protected bandgap in Fig. 2(c). Since these edge modes are in the bandgap, waves cannot scatter into the bulk of the structure and instead propagate only along the edges. Note that, all the parameters in this work (i.g.,  $m_j$ ,  $k_j$ ) are chosen to have gapless topological interface curves-see Supplementary Note 2 for more details.

# D. Topologically protected interface waves propagating along desired trajectories

A unique benefit of the proposed topological insulator is its ability to carry information along desired interface trajectories without back-scattering. To illustrate the propagation of protected waves along an interface, a *finite* plate composed of  $10 \times 10$  hexagonal unit cells is considered. To demonstrate this benefit, different interfaces (Fig. 4) are introduced between two domains, where the sign of spin-orbit coupling is reversed (i.e., op-

posite spin Chern numbers) for each domain. An harmonic force with frequency  $f = 2\pi\omega$  excites the structure from the right side. To show the energy dependency of the proposed structure, Fig. 4(a)-(b) demonstrate the displacement field of the system with a horizontal domain interface with excitation at 1.35 Hz for two different force amplitudes. Fig. 4(a) plots the wave propagation at f = 1.35 Hz with the force magnitude of (F = 1N), where at this amplitude f = 1.35 Hz lies on a dispersion curve belonging to the bulk bands. This figure clearly indicates that for the considered value of force excitation (F = 1N), bulk modes are now excited (see Fig. 2(b)), and thus waves propagate in the interior. On the contrary, Fig. 4(b) displays the displacement field of the same structure under the force magnitude of (F = 100N), clearly showing waves traveling along the domain interface from the input on the left-side, to the output on the right-side. The second example is a Z-shaped interface along the lattice vector by altering the locations of nonlinear resonators. Figure 4(c) depicts the displacement field at  $f = 1.35 \ Hz$  and F = 100N, documenting a complete transmission of the helical edge modes. Finally, Fig. 4(d) exhibits the displacement field of a triangular trajectory at f = 1.35 Hz and F = 100N, again showing transmission along the interface without back-scattering. As observed, for all of these examples, robustness of the system is guaranteed since the spin of the two edge states at the interface is locked to their respective propagation direction.

### II. CONCLUSION

In summary, this letter presented a tunable topological insulator for mechanical waves which intrinsically opens a topological bandgap using nonlinear elements. For the proposed system, the unit cell is composed of six masses connected using linear springs, where in addition three of the masses are attached to resonating masses using nonlinear stiffness to break inversion symmetry. Numerical simulations illustrate topologically-protected wave propagation, free of backscattering, along arbitrary interfaces of adjoined materials characterized by opposite spin-orbital coupling. Such a mechanical topological insulator could be an advantageous platform for implementing multiplexing, de-multiplexing, and mechanical logic in engineered systems.

#### ACKNOWLEDGMENTS

The authors would like to acknowledge Dr. Jihong Ma at Oak Ridge National Laboratory for valuable discussions. Also, the authors would like to thank the National Science Foundation for support of this research under an Emerging Frontiers in Research and Innovation (EFRI) Grant No. 1741565.

- L. Lu, J. D. Joannopoulos, and M. Soljačić, Nature Photonics 8, 821 (2014).
- [2] M. Z. Hasan and C. L. Kane, Reviews of Modern Physics 82, 3045 (2010).
- [3] X.-L. Qi and S.-C. Zhang, Reviews of Modern Physics 83, 1057 (2011).
- [4] K. Von Klitzing, Reviews of Modern Physics 58, 519 (1986).
- [5] C. L. Kane and E. J. Mele, Physical review letters 95, 226801 (2005).
- [6] F. Haldane and S. Raghu, Physical review letters 100, 013904 (2008).
- [7] Z. Wang, Y. Chong, J. D. Joannopoulos, and M. Soljačić, Physical review letters 100, 013905 (2008).
- [8] A. B. Khanikaev, S. H. Mousavi, W.-K. Tse, M. Kargarian, A. H. MacDonald, and G. Shvets, Nature materials 12, 233 (2013).
- [9] M. Hafezi, S. Mittal, J. Fan, A. Migdall, and J. Taylor, Nature Photonics 7, 1001 (2013).
- [10] V. Vitelli, N. Upadhyaya, and B. G.-g. Chen, arXiv preprint arXiv:1407.2890 (2014).
- [11] S. H. Mousavi, A. B. Khanikaev, and Z. Wang, Nature communications 6, 8682 (2015).
- [12] R. Süsstrunk and S. D. Huber, Science 349, 47 (2015).
- [13] R. Fleury, D. L. Sounas, C. F. Sieck, M. R. Haberman, and A. Alù, Science 343, 516 (2014).
- [14] C. Kane and T. Lubensky, Nature Physics 10, 39 (2014).

- [15] J. Paulose, B. G.-g. Chen, and V. Vitelli, Nature Physics 11, 153 (2015).
- [16] D. Z. Rocklin, B. G.-g. Chen, M. Falk, V. Vitelli, and T. Lubensky, Physical review letters 116, 135503 (2016).
- [17] O. Stenull, C. Kane, and T. Lubensky, Physical review letters 117, 068001 (2016).
- [18] O. R. Bilal, R. Süsstrunk, C. Daraio, and S. D. Huber, Advanced Materials 29, 1700540 (2017).
- [19] E. Prodan, K. Dobiszewski, A. Kanwal, J. Palmieri, and C. Prodan, Nature communications 8, 14587 (2017).
- [20] T. Kariyado and Y. Hatsugai, Scientific reports 5, 18107 (2015).
- [21] A. B. Khanikaev, R. Fleury, S. H. Mousavi, and A. Alù, Nature communications **6**, 8260 (2015).
- [22] J. Vila, R. K. Pal, and M. Ruzzene, Physical Review B 96, 134307 (2017).
- [23] E. Prodan and C. Prodan, Physical review letters 103, 248101 (2009).
- [24] Y.-T. Wang, P.-G. Luan, and S. Zhang, New Journal of Physics 17, 073031 (2015).
- [25] P. Wang, L. Lu, and K. Bertoldi, Physical review letters 115, 104302 (2015).
- [26] L. M. Nash, D. Kleckner, A. Read, V. Vitelli, A. M. Turner, and W. T. Irvine, Proceedings of the National Academy of Sciences 112, 14495 (2015).
- [27] R. Chaunsali, E. Kim, A. Thakkar, P. G. Kevrekidis, and J. Yang, Physical review letters 119, 024301 (2017).

- [28] R. Chaunsali, F. Li, and J. Yang, Scientific reports  ${\bf 6}$ , 30662 (2016).
- [29] R. Fleury, A. B. Khanikaev, and A. Alu, Nature communications 7, 11744 (2016).
- [30] N. Swinteck, S. Matsuo, K. Runge, J. Vasseur, P. Lucas, and P. A. Deymier, Journal of Applied Physics 118, 063103 (2015).
- [31] L. D. Landau, J. Bell, M. Kearsley, L. Pitaevskii, E. Lifshitz, and J. Sykes, *Electrodynamics of continuous me*dia, Vol. 8 (elsevier, 2013).
- [32] C. He, X. Ni, H. Ge, X.-C. Sun, Y.-B. Chen, M.-H. Lu, X.-P. Liu, and Y.-F. Chen, Nature Physics 12, 1124 (2016).
- [33] R. Chaunsali, C.-W. Chen, and J. Yang, Physical Review B 97, 054307 (2018).
- [34] R. K. Pal and M. Ruzzene, New Journal of Physics 19, 025001 (2017).
- [35] C. He, Z. Li, X. Ni, X.-C. Sun, S.-Y. Yu, M.-H. Lu, X.-P. Liu, and Y.-F. Chen, Applied Physics Letters 108, 031904 (2016).
- [36] S. D. Huber, Nature Physics **12**, 621 (2016).
- [37] R. K. Pal, M. Schaeffer, and M. Ruzzene, Journal of Applied Physics 119, 084305 (2016).
- [38] Y. Hatsugai, Physical review letters 71, 3697 (1993).
- [39] F. Zhang, A. H. MacDonald, and E. J. Mele, Proceedings of the National Academy of Sciences 110, 10546 (2013).
- [40] Z.-G. Chen and Y. Wu, Physical Review Applied 5, 054021 (2016).
- [41] Z. Zhang, Y. Tian, Y. Cheng, Q. Wei, X. Liu, and J. Christensen, Physical Review Applied 9, 034032

- (2018).
- [42] Q. Zhang, Y. Chen, K. Zhang, and G. Hu, Extreme Mechanics Letters (2019).
- [43] A. Darabi and M. Leamy, JASA (2019).
- [44] D. Dobrykh, A. Yulin, A. Slobozhanyuk, A. Poddubny, and Y. S. Kivshar, Physical review letters 121, 163901 (2018).
- [45] Y. Hadad, J. C. Soric, A. B. Khanikaev, and A. Alù, Nature Electronics 1, 178 (2018).
- [46] R. K. Narisetti, M. J. Leamy, and M. Ruzzene, Journal of Vibration and Acoustics 132, 031001 (2010).
- [47] M. D. Fronk and M. J. Leamy, Journal of Sound and Vibration 447, 137 (2019).
- [48] K. Manktelow, M. J. Leamy, and M. Ruzzene, Wave Motion 50, 494 (2013).
- [49] K. L. Manktelow, M. J. Leamy, and M. Ruzzene, Wave Motion 51, 886 (2014).
- [50] R. K. Pal, J. Vila, M. Leamy, and M. Ruzzene, Physical Review E 97, 032209 (2018).
- [51] R. Chaunsali and G. Theocharis, arXiv preprint arXiv:1904.09466 (2019).
- [52] S. Nanthakumar, X. Zhuang, H. S. Park, C. Nguyen, Y. Chen, and T. Rabczuk, Journal of the Mechanics and Physics of Solids 125, 550 (2019).
- [53] Z. Yu, Z. Ren, and J. Lee, Scientific reports 9, 1805 (2019).
- [54] B. I. Halperin, Physical Review B 25, 2185 (1982).
- [55] T. Ma and G. Shvets, New Journal of Physics 18, 025012 (2016).